VCAM-1 Upregulation Contributes to Insensitivity of Vemurafenib in BRAF-Mutant Thyroid Cancer

Shitu Chen [*,†,1], Xingyun Su [*,1], Xiaoxia Jiang [*,†], Tuo Zhang [‡], Irene Min [§], Yongfeng Ding [*], Xumeng Wang [*,†], Zhuochao Mao [*], Jiang Cao [‖], Xiaodong Teng [¶], Thomas J. Fahey III [§], Weibin Wang [*] and Lisong Teng [*,†]

[*]Cancer Center, First Affiliated Hospital, School of Medicine, Zhejiang University, Hangzhou, Zhejiang, China; [†]Key Laboratory of Precision Diagnosis and Treatment for Hepatobiliary and Pancreatic Tumor of Zhejiang Province, First Affiliated Hospital, School of Medicine, Zhejiang University, Hangzhou, Zhejiang, China; [‡]Genomic Core, Weill Cornell Medical College, New York, NY, USA; [§]Department of Surgery, New York Presbyterian Hospital and Weill Medical College of Cornell University, New York, NY, USA; [‖]Clinical Research Center, Second Affiliated Hospital, School of Medicine, Zhejiang University, Hangzhou, Zhejiang, China; [¶]Department of Pathology, First Affiliated Hospital, School of Medicine, Zhejiang University, Hangzhou, Zhejiang, China

Abstract

Vemurafenib, an inhibitor of mutant BRAF activity, is a promising anticancer agent for patients with BRAF-mutant metastatic melanoma. However, it is less effective in BRAF-mutant thyroid cancer, and the reason for this discrepancy is not yet fully elucidated. By RNA sequencing analysis, we identified vascular cell adhesion molecular-1 (VCAM-1) to be highly upregulated in both time- and dose-dependent manners during BRAF inhibition (BRAFi) in a BRAF-mutant papillary thyroid cancer cell line (BCPAP). Cell cytotoxicity and apoptosis assays showed that knockdown of the induced VCAM-1 in BCPAP cells augmented the antitumor effects of vemurafenib, with decreased IC50 values of 1.4 to 0.8 µM. Meanwhile, overexpression of VCAM-1 in a BRAF-mutant anaplastic thyroid cancer cell line (FRO) reduced the sensitivity to vemurafenib, with increased IC50 values of 1.9 to 5.8 µM. Further investigation showed that PI3K-Akt-mTOR pathway was activated during BRAFi. Co-treatment with Akt signaling inhibitor MK2206 decreased the induced expression of VCAM-1 during BRAFi. This combination further improved the efficacy of vemurafenib. Moreover, VCAM-1 promoted migration and invasion in thyroid cancer cells *in vitro*, which was also indicated in thyroid cancer patients. The present study is the first to demonstrate that VCAM-1 is upregulated in thyroid cancer cells treated with vemurafenib and

contributes to vemurafenib resistance in BRAF-mutant thyroid cancer cells. Targeting the PI3K-Akt-mTOR pathway—mediated VCAM-1 response may be an alternative strategy to sensitize BRAF-mutant thyroid cancers to vemurafenib.

Translational Oncology (2020) 13, 441–451

Introduction

Thyroid carcinoma is the most common endocrine malignancy worldwide, and its incidence in the United States has increased dramatically as the fifth most frequent neoplasm of women [1]. Differentiated thyroid cancer (DTC) is generally well behaved with favorable survival [2]. However, DTCs with tumor recurrence, distant metastases, or resistance to radioactive iodine therapy remain difficult to treat. Furthermore, poorly DTC and anaplastic thyroid carcinoma (ATC) continue to be aggressive tumors and have a high risk of death [3—5].

Mutation of an amino acid substitution at position 600 in BRAF, from a valine (V) to a glutamic acid (E) ($BRAF^{V600E}$), is the most prevalent molecular event in thyroid cancer. $BRAF^{V600E}$ is observed in 60—70% of papillary thyroid carcinoma (PTC) and 45% of ATC, and the incidence is even higher in recurrent or metastatic PTC [5,6]. In melanoma, another tumor with a high prevalence of $BRAF^{V600E}$ mutation, vemurafenib, a selective BRAF inhibitor, has demonstrated a favorable response rate of approximately 60%—80% in patients with unresectable metastatic melanoma [7]. Clinical trials of vemurafenib in thyroid carcinoma have also demonstrated antitumor effects in patients with $BRAF^{V600E}$-mutant metastatic or unresectable PTCs refractory to radioactive iodine [8,9]. However, the overall response rate for vemurafenib in thyroid carcinoma is much lower (29%) compared with $BRAF^{V600E}$-positive melanoma and other $BRAF^{V600E}$-positive nonmelanoma cancers including non—small-cell lung cancer, Erdheim—Chester disease, and Langerhans cell histiocytosis [10].

Mirroring the discrepancy in clinical response rates to vemurafenib between BRAF-mutant thyroid carcinoma and melanoma, the majority of thyroid cancer cell lines demonstrate decreased sensitivity to vemurafenib *in vitro* [11]. Coexistence with other mutations, reactivation of MAPK signaling, and activation of alternative signaling pathways including phosphatidylinositol 3-kinase (PI3K)/ Akt signaling and HER2/HER3 signaling may be responsible for BRAF inhibition (BRAFi) resistance in thyroid malignancy [12,13]. In addition, we previously reported that endoplasmic reticulum stress response—mediated autophagy could trigger drug resistance to vemurafenib [14]. Still, further investigation to elucidate the underlying mechanisms of BRAFi resistance and to identify novel therapeutic strategies to overcome the resistance is critically needed.

Several cell adhesion molecules including L1-cell adhesion molecule, intercellular adhesion molecule-1, neural cell adhesion molecule, and neuron-glia-related cell adhesion molecule have been implicated in thyroid tumor malignant progression, metastasis, and therapy resistance [15—19]. Vascular cell adhesion molecular-1 (VCAM-1), also widely known as CD106, is a member of the immunoglobulin superfamily of proteins. The soluble form of VCAM-1 has been detected in various malignancies and could be negatively associated with favorable prognosis and cancer-free survival [20—23]. VCAM-1 has also been shown to be significantly correlated with aggressive tumor behavior in thyroid cancer [24]. Furthermore, VCAM-1 could function as an indicator of responsiveness to chemotherapy and increased expression of VCAM-1 may result in chemoresistance in breast and ovarian cancer [25,26].

To date, the role of VCAM-1 during BRAFi and carcinogenesis of thyroid cancer has not yet been investigated. In the present study, we initially found that VCAM-1 was induced during BRAFi in thyroid cancer cells. We further investigated the role of induced VCAM-1 expression during BRAFi in thyroid cancer cells. Finally, we examined the underlying molecular pathway involved in VCAM-1 upregulation, as well as the potential contribution of VCAM-1 to malignant behavior in thyroid tumors.

Materials and Methods

Cell Lines and Tissue Samples

BCPAP (PTC cell line) and FRO (ATC cell line) which both harbored $BRAF^{V600E}$ mutation were used in this study. The BCPAP cell line was purchased from DSMZ (Braunschweig, Germany). The FRO cell line was generously gifted by Dr. James A. Fagin (Memorial Sloan—Kettering Cancer Institute, New York, USA). Cell line authentication was verified by short tandem repeat profiling and by BRAF mutational status analysis using sanger sequencing (Supplementary Figure 1). Both cell lines were cultured in RPMI-1640 (Gibco, Rockville, MD, USA) supplemented with 10% fetal bovine serum (FBS) and 1% penicillin/streptomycin in 5% CO_2 at 37 °C.

A total of 50 thyroid carcinoma tissue samples and matched normal tissue samples were collected from patients of the First Affiliated Hospital of Zhejiang University, who were initially diagnosed with thyroid cancer based on histopathology. All the patients provided written informed consent before surgical resection, and the protocol was approved by the Ethics Committee of the First Affiliated Hospital, College of Medicine, Zhejiang University (2018-381, 24 February 2018). Tumor staging was determined according to the 8th edition of the American Joint Committee on Cancer staging system.

Reagents and Antibodies

The BRAF inhibitor vemurafenib (PLX4032), AKT inhibitor MK2206, and MEK inhibitor U0126 were all obtained from Selleck Chemicals (Houston, TX, USA). The reactive oxygen species (ROS) inhibitor NAC (N-acetyl-L-cysteine) was purchased from Beyotime (Shanghai, China). PLX4032 and U0126 were both dissolved in dimethylsulfoxide (DMSO) in 50 mM stock. MK22062 was dissolved in DMSO in 20 mM stock. NAC was dissolved in water in 50 mM stock. Primary antibodies were used as follows: anti-VCAM-1 was obtained from Abcam (Cambridge, UK), anti-ERK, anti-phospho-ERK1/2 (Thr202/Tyr204), anti-AKT, anti-phospho-AKT (Ser473), anti-mTOR, anti-phospho-mammalian

target of rapamycin (mTOR), anti-cleaved caspase-3, anti-cleaved poly (ADP-ribose) polymerase (PARP), anti-Bim, anti-Bcl-xl, anti-Mcl-1, anti-Vimentin, anti-Snail, anti-ATP-binding cassette sub-family G member 2 (ABCG2), anti-CD44, anti-glyceraldehyde-3-phosphate dehydrogenase (GAPDH), and horseradish peroxidase (HRP)-conjugated anti-rabbit and anti-mouse secondary antibodies were all purchased from Cell Signaling Technology (Beverly, MA, USA).

RNA Extraction and Quantitative Real-Time PCR

Total RNA of each sample was isolated using RNeasy Mini Kit (Qiagen, Hilden, Germany) following the manufacturer's recommendations. RNA (1 μg) was reverse transcribed to cDNA using the PrimeScript RT reagent kit (Takara, Kyoto, Japan). qRT-PCR was carried out using a SYBR Green PCR kit (Takara, Kyoto, Japan) on the ABI StepOne Plus Realtime PCR System (Applied Biosystems, Foster City, CA, USA). Analysis of relative gene expression data was made through the $2^{-\Delta\Delta Ct}$ method, using GAPDH as a normalization control. The primers for real-time PCR were listed as followings: VCAM-1: forward 5′-AGCAACTTGTGAATCTAGGA-3′ and reverse 5′-GCAACTGAACACTTGACTG-3′; GAPDH: forward 5′-GGAGCGAGATCCCTCCAAAAT-3′ and reverse5′-GGCTGTTGTCATACTTCTCATGG-3′.

RNA Sequencing and Data Analysis

RNA sequencing of control and vemurafenib-treated BCPAP cells (each with two biological replicates) was performed using Illumina Hiseq4000 sequencing system (Weill Cornell Medical College). Illumina sequencing libraries were constructed according to a modified strand-specific RNA sequencing protocol [27]. Gene expression levels were measured using Cufflinks as previously reported [28]. The heatmaps for genes of interest were generated using R package software. These sequence data have been submitted to the GenBank database under accession number SRR8799740, SRR8799741, SRR8799742, and SRR8799743.

Western Blotting

Harvested cells were lysed in cold radioimmunoprecipitation buffer assay (Beyotime, Shanghai, China) with 1% protease inhibitor cocktail (Bioship, Hefei, Anhui, China) and 1% phosphatase inhibitors (Bioship, Hefei, Anhui, China). Equal amounts of cell protein measured by BCA Protein Assays (Thermo Fisher Scientific, Waltham, MA, USA) were separated on SDS-PAGE gels and transferred to polyvinylidene difluoride membranes (Millipore, Billerica, MA, USA). After blocked in 10% skim milk in TBS-T (10 mM Tris−HCl [pH 7.5], 0.5 M NaCl, and 0.05% [w/v] Tween 20) at room temperature for 1 hour, the membranes were then probed with primary antibodies overnight at 4 °C. The next day, the membranes were incubated with HRP-linked secondary antibodies for 1 hour at room temperature. GAPDH was probed to verify equal protein loading. Blots were visualized by an enhanced chemiluminescence (ECL) detection system (ECL Plus, Millipore, Billerica, MA, USA). The intensities of bands were quantified by ImageJ densitometric analysis (National Institutes of Health, Bethesda, MD, USA).

RNA Interference

VCAM-1 small interfering RNAs (siRNA-VCAM-1) and non-target small interfering RNA (siRNA-NT) were purchased from RiboBio Company (Guangzhou, Guangdong, China). Transfection was performed using Lipofectamine 3000 transfection reagent (Invitrogen, Carlsbad, CA, USA) in Opti-MEM medium (Gibco, Rockville, MD, USA) following the manufacturer's instructions. Cells were exposed to vemurafenib 24 hours after transfection. The siRNAs target sequences were as follows: si-VCAM-1-#1, sense, 5′-GCAGAAAGGAAGUGGAAUU-3′, antisense, 5′-AAUUCCACUUCCUUUCUGC-3′; si-VCAM-1-#2, sense, 5′-AAUGCAACUCUCACCUUAA-3′, antisense, 5′-UUAAGGUGAGAGUUGCAUU-3′.

Lentivirus Infections

Recombinant lentivirus (pLenti-EF1a-EGFP-P2A-Puro-CMV-VCAM1-3FLAG) and control vector (as negative control) were constructed by Obio Technology (Shanghai, China). The DNA sequence of VCAM-1 was obtained from GenBank (NM_001078). For lentivirus infection, 1×10^{5} cells were seeded in 24-well plate and infected with recombinant lentivirus or control vector. Virus-infected cells harbored positive green fluorescence GFP protein and were selected with 2 μg/mL puromycin (Genechem, Shanghai, China). The antibiotic-resistant clones were survived and collected for subsequent studies.

Assessment of ROS Levels

ROS levels were determined by staining cells with the fluorescent probe 2,7-dichlorofluorescein diacetate (DCFH-DA, Beyotime, Shanghai, China) using flow cytometry. The cells were initially stained with 10 μM DCFH-DA for 30 min at 37 °C. After completely removing DCFH-DA, 1×10^{6} cells were treated with vemurafenib, DMSO, positive control for 2 hours. The cells were kept in the dark on ice and at least 10,000 cells for each sample were analyzed using flow cytometer BD FACSCanto II (BD Bioscience, San Jose, CA, USA). And then ROS generation was measured by the fluorescence intensity (FL-1,530 nm) of 10,000 cells.

Cell Apoptosis Assays

An Annexin V-fluorescein isothiocyanate (FITC)/propidium iodide (PI) detection kit (BD Bioscience, San Jose, CA, USA) was used following the manufacturer's instructions. After exposed to indicated treatments for 24 hours, cells were collected and resuspended in binding buffer, followed by incubation with FITC and PI in dark for 15 min. Stained cells were detected by flow cytometer FACSCanto II (BD Bioscience, San Jose, CA, USA). FlowJo software (Version X, Ashland, USA) was used for data analysis.

Cell Migration, Invasion Assays

Transwell chambers of 24-well format with 8.0-μm pore size polycarbonate filter inserts (Millipore, Billerica, MA, USA) were used for examining cell migration and invasion *in vitro*. Cells were prestarved in serum-free medium overnight and resuspended in serum-free medium. For the invasion assays, 4×10^{4} cells per well were seeded in Matrigel (BD Bioscience, San Jose, CA, USA)-coated upper chamber. For the migration assays, 2×10^{4} cells per well were seeded in uncoated upper chamber. The lower chamber was filled with 900 μL medium with 10% FBS. After incubation for 48 hours at 37 °C with 5% CO_2, nonpenetrating cells on the upper side of the filter were wiped-off and penetrating cells were fixed with 95% ethanol, stained with 0.1% crystal violet, then counted in at least five random fields (100×) under a light microscope.

Wound Healing Assays

A wound was scratched by a micropipette tip before the monolayer cell overgrew. Cells were cultured in medium without FBS for 24 hours. We analyzed the images (100×) and calculated the distance between the wound sides by light microscope. The analysis of wound healing assays was performed using the ImageJ software (National Institutes of Health, Bethesda, MD, USA).

Cell Proliferation and Cytotoxicity Assays

Cell proliferation and cytotoxicity assays were carried out using cell counting kit-8 (CCK-8) (Dojindo Laboratories, Kumamoto, Japan). For cell proliferation assays, 3000 cells were seeded into 96-well plates with 100 μL full medium and incubated for 6 hours, 24 hours, 48 hours, and 72 hours. For cell cytotoxic assays, cells (5000/well) were seeded in 96-well plates and treated with chemicals at different concentrations for 72 hours. 10 μL CCK-8 reagent was added to each well for indicated time periods and incubated for another 2 hours at 37 °C. The absorbance at 450 nm wavelength was measured by a multiwell spectrophotometer (Bio-Rad, Hercules, CA, USA). IC50 values were calculated using GraphPad Prism 7.0 (GraphPad software; La Jolla, CA, USA) at least three independent experiments.

Colony-Forming Cell Assays

Cells were cultured in a six-well plate at 500 cells per well in triplicate with full media for 7—10 days. Colonies were fixed with 95% ethanol, stained with 0.1% crystal violet before quantification and photographing.

Statistics Analysis

Data were analyzed by Student unpaired, 2-tailed t-test with GraphPad Prism 7. P-values less than 0.05 were considered as statistically significant and indicated in the figures as follows: ***$P < 0.001$, **$P < 0.01$, *$P < 0.05$. Experiments were performed in triplicate and repeated at least 3 times. Results show the mean ± SD of three independent assays.

Results

VCAM-1 is Upregulated by Vemurafenib in Both Time- and Dose-Dependent Manners

Previous studies have shown that thyroid cancer cell lines were relatively insensitive to vemurafenib [11], and this finding was demonstrated again by the high concentration of vemurafenib needed to reach IC50 with BCPAP, a PTC cell line, and FRO, an ATC cell line (Supplementary Figure 2). To characterize the potential molecular events responsible for the drug insensitivity during BRAFi in thyroid cancer, we analyzed RNA expression levels by RNA-seq and identified 4757 genes that were differentially expressed by vemurafenib-treated BCPAP cells vs BCPAP cells treated with DMSO only as vehicle control for 24 hours. There were 2214 upregulated and 2543 downregulated genes after 24 hours of vemurafenib treatment in BCPAP cells. Hierarchical clustering of transcriptional profiling showed the distinguishable mRNA expression patterns between these two groups (Figure 1A). Further Kyoto Encyclopedia of Genes and Genomes (KEGG) molecular pathway analysis revealed cell adhesion molecules were differentially expressed after BRAFi. Heat map analysis showed the 9 upregulated immunoglobulin superfamily genes during BRAFi with statistical significances. Among them, VCAM-1 was the most upregulated gene with 6.43-fold change (Figure 1B).

Hence, we identified VCAM-1 as a gene of interest and set out to assess the role of induced VCAM-1 expression during BRAFi in thyroid cancer. We measured the protein expression level of VCAM-1 in thyroid cancer cells during BRAFi. Consistently, in BCPAP cells,
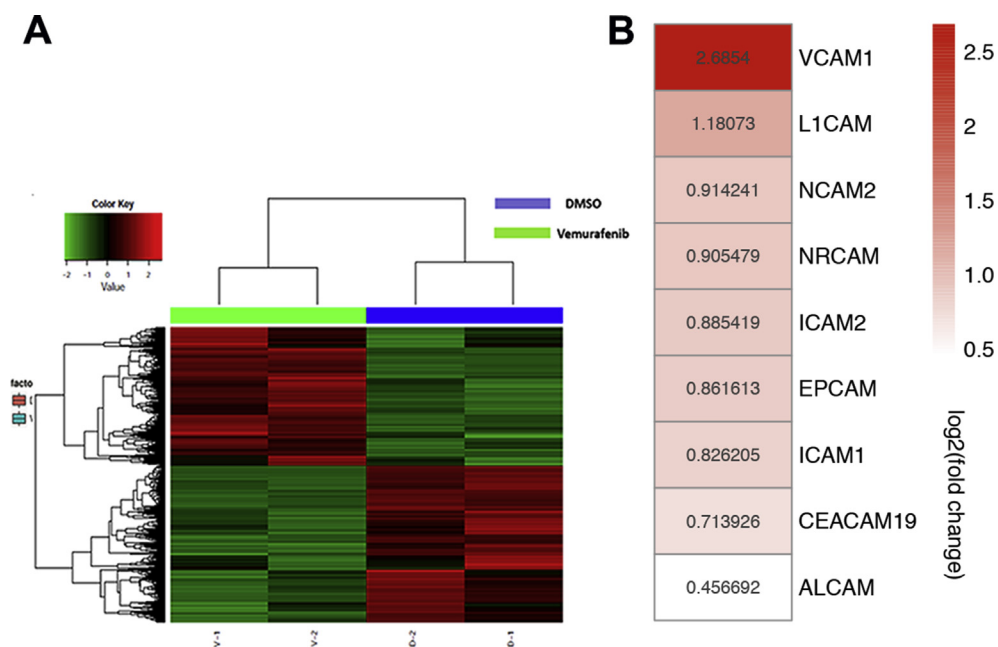
Figure 1. Transcriptional profiles of BCPAP cells after vemurafenib treatment by a high-throughput RNA sequencing. (A) Hierarchical cluster of differentially expressed mRNAs. BCPAP cells were treated either with 5 μM vemurafenib or vehicle for 24 hours. Red color indicates relative high expression and green color indicates relative low expression. (B) Heat map analysis showing the relative mRNA expression of several cell adhesion molecules. All of them were upregulated during BRAF inhibition with log2 fold change ranging from 0.46 to 2.69, among which VCAM-1 had the most remarkable change.
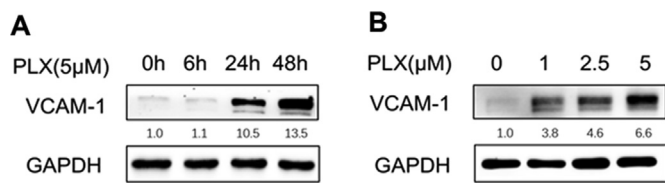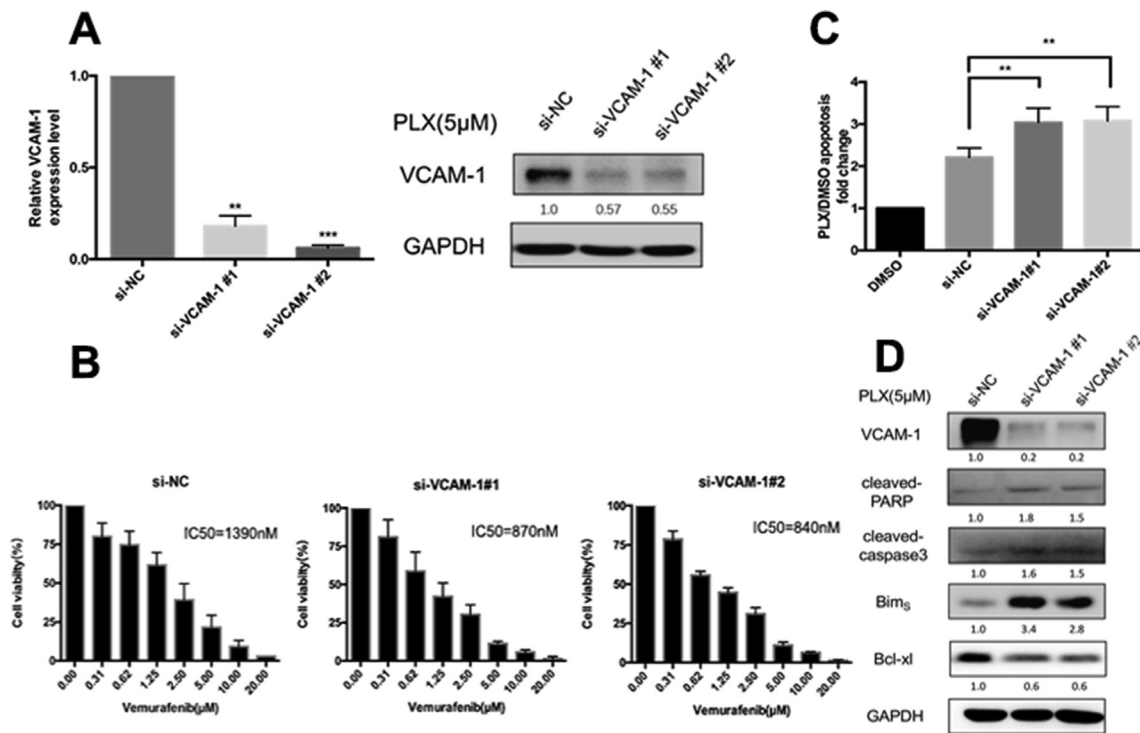
Figure 2. VCAM-1 is upregulated by vemurafenib (PLX) in BCPAP cells. (A) Vemurafenib treatment induced VCAM-1 upregulation in a time-dependent manner. BCPAP cells were treated with either DMSO or 5 µM PLX for indicated times (6 hours, 24 hours, and 48 hours). The expression of VCAM-1 was detected by western blot analysis. Relative expression level of VCAM-1 to GAPDH was calculated by ImageJ densitometric analysis and normalized to control (DMSO). (B) VCAM-1 was induced by PLX in a dose-dependent manner. BCPAP cells were exposed to indicated concentrations of PLX (1 µM, 2.5 µM, and 5 µM) for 24 hours and the expression of VCAM-1 was determined by western blotting. Relative expression level of VCAM-1 to GAPDH was calculated by ImageJ densitometric analysis and normalized to control (DMSO).

VCAM-1 expression started to increase gradually after 6-hour treatment and reached significant change by 48 hours (Figure 2A). The increase in VCAM-1 expression in BCPAP cells was also dose-related (Figure 2B). However, in the ATC cell line FRO, no VCAM-1 expression was detected even after vemurafenib treatment

(Supplementary Figure 3). We therefore used FRO cell line for establishing a VCAM-1 overexpression model for subsequent studies.

Induced VCAM-1 Facilitates the Drug Insensitivity of Vemurafenib in Thyroid Cancer Cells

To test whether the induced VCAM-1 was associated with drug insensitivity in thyroid carcinoma, we knocked down the upregulated VCAM-1 in BCPAP cells by using two independent sequences of siRNA. Decreased expression of VCAM-1 was confirmed at both mRNA and protein levels (Figure 3A). Inhibition of VCAM-1 expression markedly facilitated growth inhibition as compared with vemurafenib treatment alone, with decreased IC50 values of 1.4 to 0.8 µM (Figure 3B). Knockdown of VCAM-1 induced BCPAP apoptosis significantly when BRAF signaling was inhibited by vemurafenib (Figure 3C). Increased proapoptotic protein expressions including caspase 3 cleavage, poly ADP-ribose polymerase (PARP) cleavage, and Bim and decreased expression of antiapoptotic protein Bcl-xl were observed in BCPAP cells transfected with si-VCAM-1 when treated with PLX4032 for 24 hours as compared with PLX4032 treatment alone (the si-NC group) (Figure 3D). We next over-expressed VCAM-1 in FRO cells through recombinant lentivirus transduction (Figure 4A). Overexpressed VCAM-1 attenuated the growth inhibition effects of vemurafenib in FRO cells with increased IC50 values of 1.9 to 5.8 µM (Figure 4B). Furthermore, this

Figure 3. Downregulation of VCAM-1 sensitizes BCPAP cells to vemurafenib treatment. (A) The upregulated VCAM-1 expression by vemurafenib was significantly suppressed by siRNAs in BCPAP cells. The expression level of VCAM-1 was measured by both qRT-PCR (**: $P < 0.01$; ***: $P < 0.001$) and western blot assays. Relative expression level of VCAM-1 to GAPDH was calculated by ImageJ densitometric analysis and normalized to control (si-NC). (B) The cytotoxic effect of vemurafenib with increasing concentrations on si-NC or si-VCAM-1 transfected BCPAP cells after 72 hours exposure, as determined by CCK-8 assays. IC50 values are shown in the graphs (nmol/L). Error bars, SD from 3 independent experiments. (C) si-NC or si-VCAM-1 transfected BCPAP cells were treated with 5 µM PLX for 24 hours. The percentages of annexin-V expressed cells were determined by flow cytometry analysis and the bar graph shows the apoptosis ratio of PLX-treated transfected cells relative to DMSO-treated control cells (**: $P < 0.01$). Error bars, SD from 3 independent experiments. (D) Western blot analysis of whole cell lysates from transfected cells after 5 µM of PLX treatment for 24 hours. Membranes were probed for cleaved-caspase 3, cleaved-PARP, Bim$_S$, and Bcl-xl. Relative expression levels of indicated antibodies were calculated by ImageJ densitometric analysis and normalized to control (si-NC).
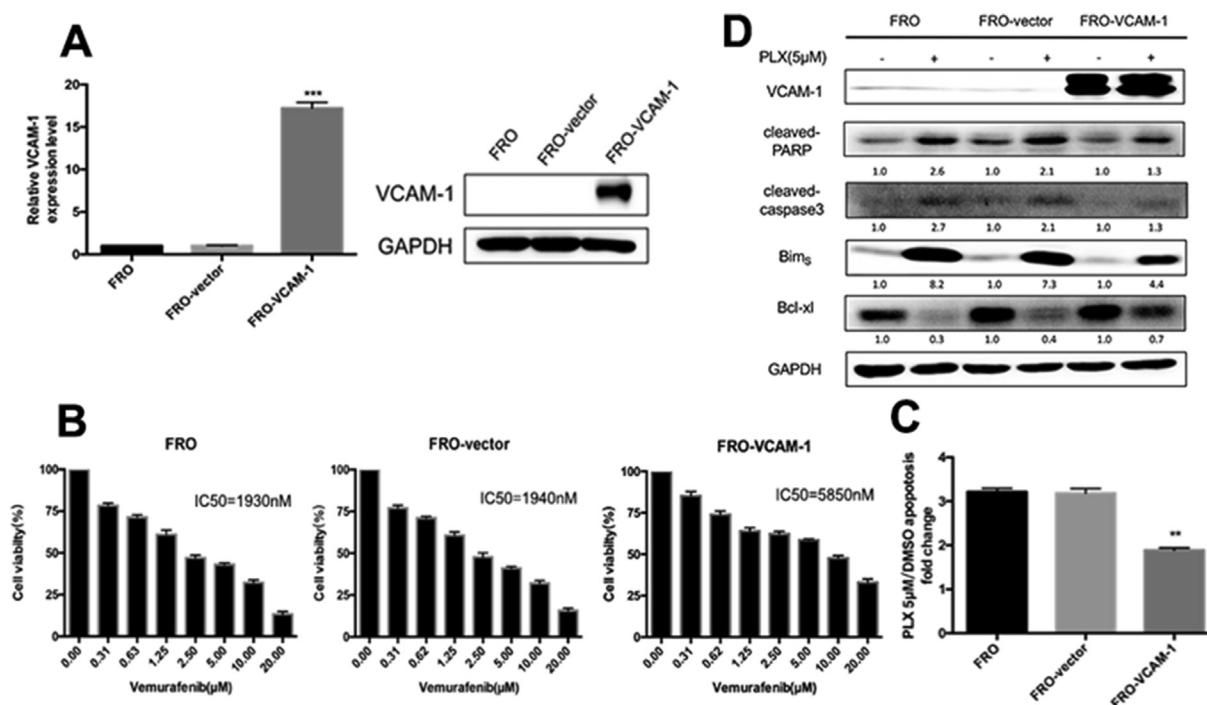
Figure 4. The overexpression of VCAM-1 promotes thyroid cancer insensitivity to vemurafenib in FRO cells. (A) The overexpression cell model of VCAM-1 was constructed by transducing the FRO cells with the recombinant lentivirus expressing VCAM-1 (FRO-VCAM-1). The expression level of VCAM-1 was measured by both qRT-PCR (***: $P < 0.001$) and western blot assays. (B) The cytotoxic effects of vemurafenib with increasing concentrations on FRO cells, FRO cells transfected with empty vector (FRO-vector), and FRO-VCAM-1 cells after 72 hours exposure were determined by CCK-8 assays. IC50 values are shown in the graphs (nmol/L). Error bars, SD from 3 independent experiments. (C) To determine the apoptosis ratio relative to DMSO-treated controls, the percentages of annexin-V expressed cells were analyzed by flow cytometry in FRO, FRO-vector, FRO-VCAM-1 cells cells treated with 5 μM of PLX for 24 hours. The bar graph shows the apoptosis ratio of PLX treatment groups and DMSO treatment groups for three cells (**: $P < 0.01$). Error bars, SD from 3 independent experiments. (D) Western blot analysis of whole cell lysates from FRO, FRO-vector, and FRO-VCAM-1 cells exposed to 5 μM PLX for 24 hours. Membranes were probed for cleaved-caspase 3, cleaved-PARP, Bim_S, and Bcl-xl. Relative expression levels of indicated antibodies in FRO, FRO-vector, and FRO-VCAM-1 cells were calculated by ImageJ densitometric analysis and normalized to control (DMSO), respectively.
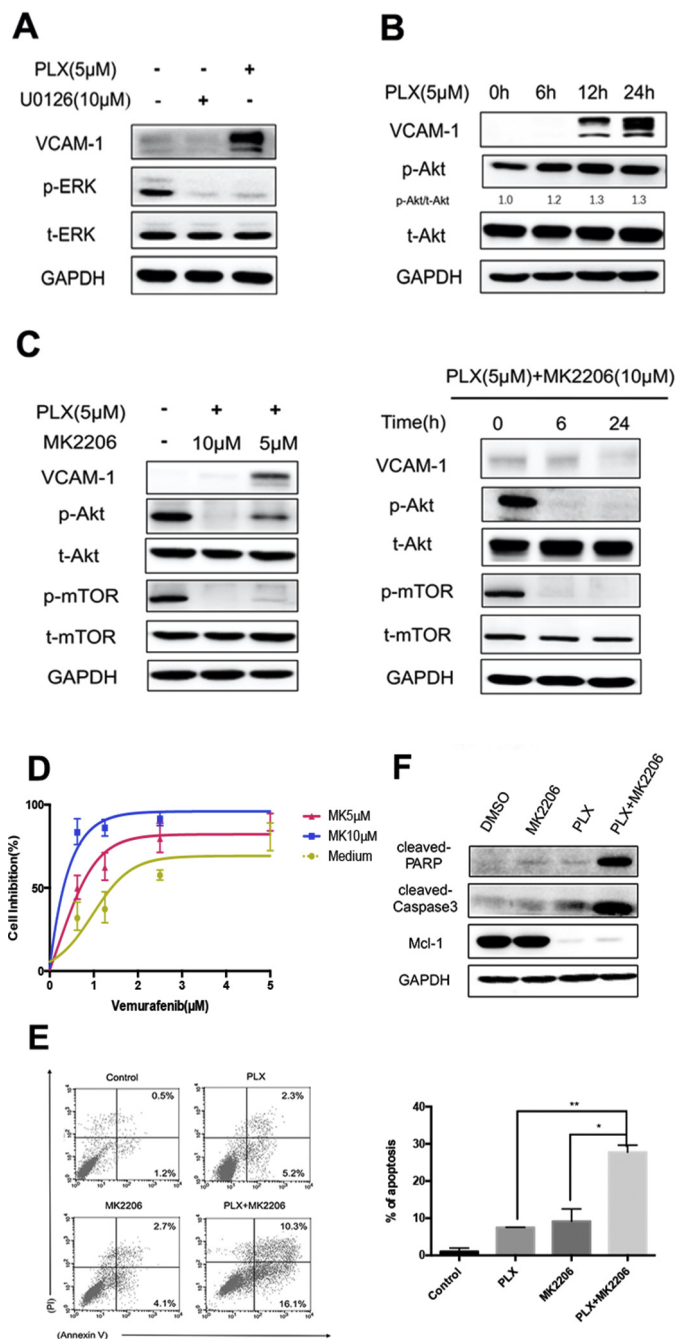
attenuation was accompanied by the decreased level of apoptosis, reduced expression of proapoptotic proteins including cleaved caspase-3, cleaved PARP, and Bim, and increased expression of antiapoptotic protein Bcl-xl (Figures 4C and D). Meanwhile, the expressions of apoptosis-related proteins by western blotting analysis and apoptotic levels by flow cytometer had little difference among FRO, FRO-vector, and FRO-VCAM-1 cells (Supplementary Figure 4). Taken together, these results demonstrate that the cell growth inhibitory effects of decreased VCAM-1, in conjunction with PLX4032 treatment, are mediated mainly by the Bcl-2 family proteins and caspase-dependent apoptosis pathways.

Reversion of the upregulated VCAM-1 expression by Akt inhibitor sensitizes BRAF-mutant thyroid cancer to vemurafenib.

To investigate the possible signaling pathways that mediate VCAM-1 upregulation, we first checked whether vemurafenib-induced VCAM-1 expression was MAPK pathway dependent. By comparing the effect of vemurafenib with U0126, a specific inhibitor of MEK1 and MEK2, we found that ERK phosphorylation was completely inhibited after 24 hours of treatment in BCPAP cells by both 5 μM vemurafenib and 10 μM U0126 (Figure 5A). However, the expression of VCAM-1 was not increased during MAPK signaling pathway inhibition by U0126, suggesting that vemurafenib-induced VCAM-1 upregulation was independent of MAPK signaling pathway (Figure 5A).

VCAM-1 expression could be stimulated by high levels of ROS, Akt, and NF-κB signaling [29–31], which were also reported to be involved in vemurafenib resistance of thyroid cancer [32–35]. Here we found that phosphorylation of Akt was upregulated after 5 μM vemurafenib treatment for indicated time intervals in BCPAP cells (Figure 5B). To determine whether VCAM-1 upregulation during BRAFi resulted from persistently activated phosphorylated Akt, BCPAP cells were exposed to a combination of 5 μM vemurafenib and 10 μM MK2206, a specific Akt1/2/3 inhibitor, for 24 hours. Notably, inhibition of phospho-Akt with MK2206 abrogated the induction of upregulated VCAM-1 during BRAFi by 24 hours (Figure 5C). More complete suppression of VCAM-1 expression was observed in cells treated with 10 μM MK2206 than 5 μM drug concentration, suggesting a role for Akt signaling as the major mediator of VCAM-1 in BCPAP cells during BRAFi (Figure 5C). To further investigate the association between VCAM-1 upregulation and Akt signaling pathway, we detected ROS production by flow cytometry. Vemurafenib triggered ROS production by 2.0-fold change. The ROS generation was decreased when combined treatment with a ROS inhibitor NAC. However, the dual blockade of ROS generation and BRAF did not inhibit the expression of VCAM-1, suggesting

that the upregulation of VCAM-1 do not result from excess ROS generation (Supplementary Figure 5).

Then we evaluated the cytostatic activity of cotreatment with PLX4032 and MK2206 in BCPAP cells. Relative to vemurafenib-treated groups, the combined blockade of Akt and BRAF resulted in much greater cell growth inhibition by 24 hours (Figure 5D). After dual treatment with 5 μM MK2206, the IC50 value of PLX was 660 nM. Additive cytotoxicity was produced by a higher dose of MK2206 (10 μM) with an IC50 value of 23 nM. In addition, 5 μM PLX4032 or 10 μM MK2206 alone induced only modest apoptosis of BCPAP cells; however, their combination markedly increased apoptosis by 3.49-fold (Figure 5E). Consistently, under the cotreatment of 10 μM MK2206 and 5 μM PLX4032 for 24 hours, the protein levels of the apoptosis markers cleaved caspase-3 and cleaved PARP were elevated and antiapoptotic protein Mcl-1 was notably inhibited (Figure 5F).

VCAM-1 Plays a Role in Tumor Invasion and Metastasis in Thyroid Cancer

To study the biological function of VCAM-1 in thyroid cancer cells, we initially performed CCK-8 and clonogenetic assays for cell proliferation assessment in FRO cells. No significant difference was detected between VCAM-1 overexpression groups and control groups (Figures 6A and B). However, wound healing assays and transwell assays showed that overexpression of VCAM-1 in FRO cells increased cell migration and invasion ability (Figures 6C and D). Furthermore, we demonstrated that FRO-VCAM-1 cells had increased expression of Vimentin and Snail, which was related to epithelial−mesenchymal transition (EMT). CD44 and ABCG2, markers of cancer stem cells, were also detected with elevated expression in FRO-VCAM-1 cells. Meanwhile, knockdown of the upregulated VCAM-1 during BRAFi decreased the expressions of them, indicating that VCAM-1 may be facilitating cell mobility via EMT or stemness (Figure 6E).

To evaluate the correlation between VCAM-1 and clinical pathological features, we analyzed the mRNA expression level of VCAM-1 in 50 PTC patients. Although there was no significant expression difference between tumor and normal tissues ($P = 0.0549$), our data showed that VCAM-1 mRNA expression in PTC patients was higher in those with lymph node metastasis compared with localized disease ($P = 0.026$, Figure 6F). These data suggest that overexpression of VCAM-1 may be associated with

Figure 5. Inhibition of upregulated VCAM-1 by Akt inhibitor MK2206 sensitizes BCPAP to vemurafenib. (A) Vemurafenib induced VCAM-1 expression independently of MAPK signaling pathway. BCPAP cells were treated with either PLX (5 μM) or U0126 (10 μM) for 24 hours, after which whole-cell protein lysates were subjected to western blotting assays with the indicated antibodies. (B) Vemurafenib elevated VCAM-1 expression and phosphorylation of Akt. BCPAP cells were treated with 5 μM of PLX for indicated times (6 hours, 12 hours, and 24 hours), after which whole-cell protein lysates were subjected to western blotting assays with the indicated antibodies. Relative expression level of p-Akt/t-Akt was calculated by ImageJ densitometric analysis and normalized to control (DMSO). (C) Cotreatment with Akt inhibitor MK2206 could reverse the upregulation of VCAM-1 during BRAF in both time- and dose-dependent ways. BCPAP cells were treated with 5 μM of PLX and 5 μM of MK2206 or 10 μM of MK2206 for 24 hours or treated with 5 μM of PLX and 10 μM of MK2206 for indicated times (6 hours, 24 hours), after which whole-cell protein lysates were subjected to western blotting assays with the indicated antibodies. (D) Cell viability assays of 5 μM of PLX treatment alone or combined either with 5 μM of MK2206 or 10 μM of MK2206 were detected after 24 hours treatment using CCK-8 reagent in BCPAP cells. Error bars, SD from 3 independent experiments. The IC50 values of PLX alone, PLX combined 5 μM of MK2206, and 10 μM of MK2206 were 1460 nM, 660 nM, and 23 nM, respectively. (E) Apoptotic levels in BCPAP cells treated with 5 μM PLX alone or together with 10 μM MK2206 were determined by flow cytometer. The bar graph in the right panel presents quantitative analysis of apoptosis cells in 4 different treatment groups (*: $P < 0.05$; **: $P < 0.01$). Error bars, SD from 3 independent experiments. (F) Western blot analysis of whole-cell lysates from BCPAP cells exposed to either 10 μM MK2206 or 5 μM PLX or a combination. Membranes were probed for cleaved-caspase 3, cleaved-PARP, and Mcl-1. p-, phospho-; t-, total.
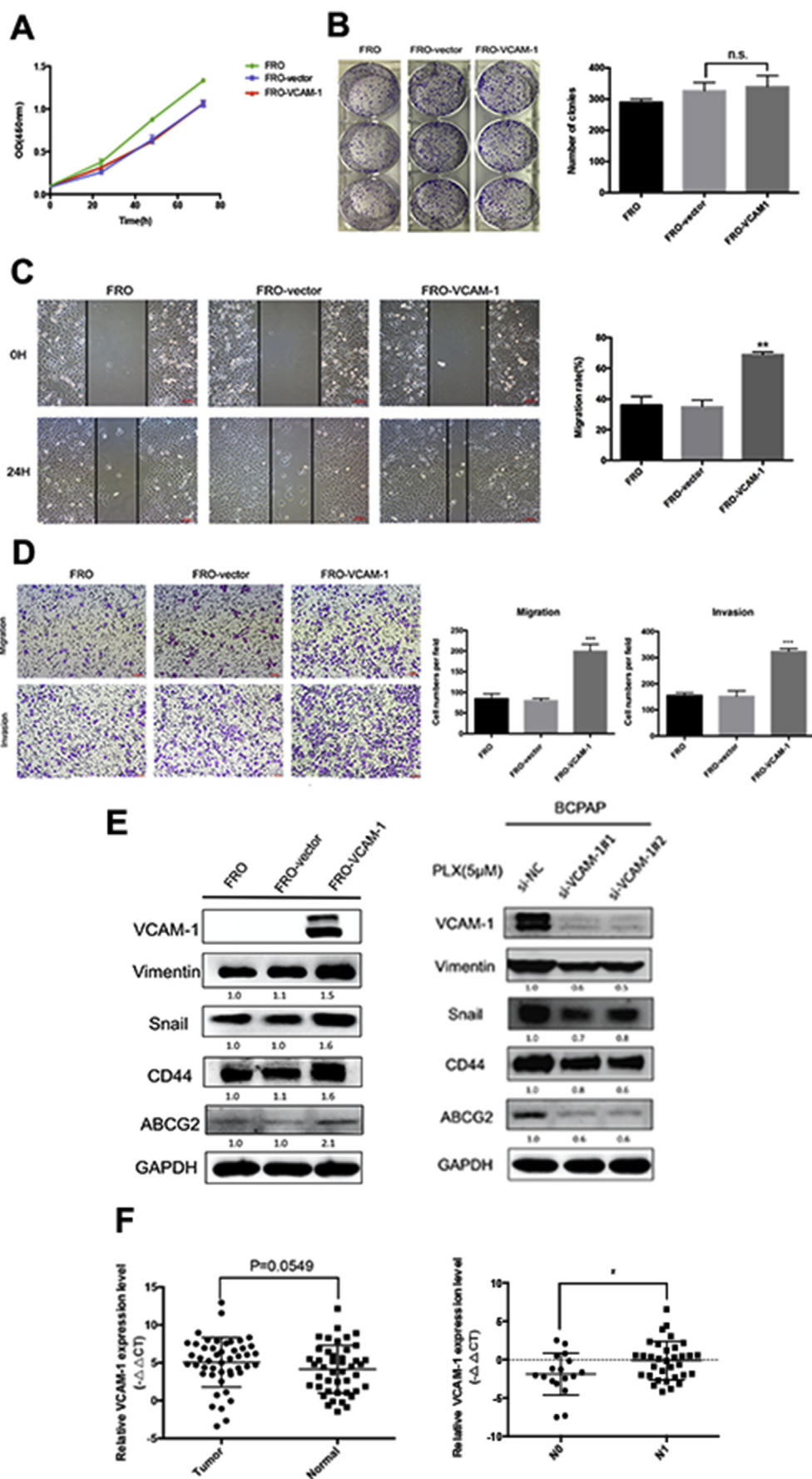
enhanced invasion and migration ability *in vivo*, consistent with our findings *in vitro*.

Discussion

The development of the small molecule BRAF inhibitor drugs has brought clinical benefit to BRAF-mutant cancer patients. Unfortunately, the high response rates seen in melanoma have not extended to BRAF-mutant advanced thyroid malignancies and the reasons still remain unclear. In the present study, we provide evidence that Akt-mediated upregulation of VCAM-1 during BRAFi promotes drug insensitivity in thyroid cancer. In addition, our data suggest that VCAM-1 may promote migration and invasion ability of thyroid cancer cells and is correlated with increased lymph node metastases in thyroid cancer patients.

VCAM-1 is widely expressed in activated endothelial cells, bone marrow stromal cells, and also some tumor cells [36]. It mainly functions by binding to late antigen-4 (VLA-4, α4β1) and integrin α4β7 [37] and is involved in the inflammatory response, cell differentiation, recruitment of lymphocytes, and tumorigenicity and metastasis [38].

In addition to its function as an adhesion molecule, VCAM-1 expression could reflect tumor response to chemotherapy. Research from MD Anderson showed that VCAM-1/VLA-4 triggered reciprocal NF-kB activation contributing to leukemia chemoresistance [31]. Scalici et al. demonstrated that VCAM-1 could be a sensitive indicator for peritoneal metastasis and response to platinum-based chemotherapy of ovarian cancer [26]. Wang et al. further investigated the biological functions of VCAM-1 in breast cancer and showed that overexpression of VCAM-1 enhanced a chemoresistance phenotype through increasing the expression of ABCG2 and CD44 [25]. Until now much less is known about the role of VCAM-1 during BRAFi in thyroid cancer. As shown here, knockdown or inhibition of the upregulated VCAM-1 during BRAFi enhanced the drug efficacy of vemurafenib by promoting apoptosis, while overexpression of VCAM-1 had the opposite effect. Consistent with previous data, we also found an additive increase of stemness markers ABCG2 and CD44 in FRO-VCAM-1 cells, which might partly explain the reason for drug resistance. Still, the underlying mechanism of VCAM-1 and drug sensitivity to vemurafenib is largely unknown and needs further exploration.

VCAM-1 expression could be induced by a multitude of inflammatory signals such as ROS, cytokines, high concentrations of glucose, and TLR agonists [38]. In addition, multiple signaling pathways were involved in the upregulation of VCAM-1 including PI3K/Akt, NF-κB, and Src activation [39,40]. The Akt signaling pathway has already been shown to play a crucial role in tumorigenesis of thyroid cancer. Thyroid cancer cell lines could develop resistance to vemurafenib through alternative activation of PI3K/Akt signaling pathway [41]. Accordingly, we also found that Akt inhibition enhanced BRAFi-induced cell apoptosis. In addition, accumulating evidence has shown that activation of the Akt-associated signaling pathway was related to the regulation of endothelial cell function and could upregulate the expression of VCAM-1 via ROS production [42,43]. However, we did not identify a correlation of VCAM-1 and ROS production; therefore, the upregulation of VCAM-1 by Akt signaling might be ROS independent in our study. Besides, it was reported that heterodimers of EGFR or HER2/HER3 could activate the PI3K-Akt-mTOR pathway and contribute to BRAFi resistance in thyroid cancer [13,44]. Along with the increased HER-2 expression during BRAFi (unpublished data), it was possible that the activation of HER2 promoted Akt phosphorylation and subsequently upregulated VCAM-1 expression. The present study demonstrated that Akt was an important mediator of VCAM-1 upregulation during BRAFi in thyroid cancer; however, more research is needed to explore the specific mechanism between Akt signaling and VCAM-1. Taken together, our data identify a new mechanistic link supporting the hypothesis that the Akt signaling pathway is a key factor in thyroid cancer BRAFi resistance because of its ability to induce the expression of VCAM-1 and maintain cell survival under vemurafenib treatment.

The role of aberrantly overexpressed VCAM-1 in tumor metastasis has already been partly investigated [45–47]. Rice suggested that VCAM-1 promoted adhesion of melanoma cells and affected the incidence and distribution of metastasis [48]. Further studies have shown VCAM-1/VLA-4 interaction can draw tumor-associated macrophages to cancer cells. Clustering of cell surface VCAM-1 leads to activation of Akt. Akt in turn protected cancer cells from proapoptotic cytokines and thus fostered lung metastasis of breast cancer [49]. Moreover, induction of the EMT program appears to be another reason underlying the metastatic mechanism as well [25]. Along with studies of colorectal, gastric, and ovarian cancer

Figure 6. VCAM-1 overexpression mediates migration and invasion potentials of thyroid cancer. (A) The cell viability of FRO, FRO-vector, and FRO-VCAM-1 cells were determined by CCK-8 assays. Error bars, SD from 3 independent experiments. (B) The proliferation of FRO, FRO-vector, and FRO-VCAM-1 cells by colony formation assays. The bar graph in the right panel presents quantitative analysis of colony numbers in 3 different groups (n.s.: not significant). (C) The motility of FRO, FRO-vector, and FRO-VCAM-1 cells was measured by wound healing assays. The bar graph in the right panel indicates migration rates (migration distance/original width) after 24 hours incubation in serum-free media (**: $P < 0.01$). Error bars, SD from 3 independent experiments. All images were acquired under 100× magnification (scale bar: 10 μm). (D) The migration and invasion ability of FRO, FRO-vector, and FRO-VCAM-1 cells was determined by transwell assays. The bar graph in the right panel presents quantitative analysis of migration or invasion cell number per field in 3 different groups (***: $P < 0.001$). Error bars, SD from 3 independent experiments. All images were acquired under 100× magnification. (E) Left: Western blot analysis of whole-cell lysates from FRO, FRO-vector, and FRO-VCAM-1. Membranes were probed for VCAM-1, Snail, Vimentin, CD44, and ABCG2. Relative expression levels of indicated antibodies were calculated by ImageJ densitometric analysis and normalized to control (FRO cells). Right: western blot analysis of whole-cell lysates from transfected cells after 5 μM of PLX treatment for 24 hours. Membranes were probed for VCAM-1, Snail, Vimentin, CD44, and ABCG2. Relative expression levels of indicated antibodies were calculated by ImageJ densitometric analysis and normalized to control (si-NC). (F) qRT-PCR analysis of VCAM-1 expression in matched normal and cancerous tissues (left, $P = 0.0549$) or in no lymphatic metastasis group (N0) and lymphatic metastasis group (N1) (right, *: $P < 0.05$) of 50 thyroid papillary cancer patients in our hospital. Relative expression levels of VCAM-1 were calculated and compared by $-\Delta\Delta Ct$ values.

[22,23,26], VCAM-1 expression is also markedly correlated with aggressive tumor behavior and poor prognosis in thyroid carcinoma patients [24]. Nevertheless, little was known about the biological function of VCAM-1 in thyroid cancer until now. In the present study, we found VCAM-1 overexpression regulated the EMT-related molecules, Vimentin and Snail, and also enhanced stem cell phenotype by upregulating CD44 and ABCG2, thus promoting tumor migration and invasion. Moreover, a correlative analysis of VCAM-1 expression levels in 50 thyroid cancer patients showed that higher expression of VCAM-1 was associated with a higher incidence of lymph node metastasis. These results further support the role of VCAM-1 in tumor invasion and metastasis of thyroid cancer.

As for drug evaluation, using primary human tumor cell lines *in vitro* or patient-derived tumor tissue (PDTT) xenografts *in vivo* may be more effective to test therapeutic regimens [50,51]. The results would be more significant if we tested the cytotoxic effect of combined inhibition of VCAM-1 and BRAF mutation in primary human tumor cell lines or PDTT xenografts. We have continued to establish primary thyroid cancer cell lines and PDX models for further study.

Conclusions

In summary, our data demonstrate that VCAM-1 upregulation during BRAFi contributes to vemurafenib resistance. Inhibition of VCAM-1 could be an alternative strategy to sensitize BRAF-mutant thyroid cancer to vemurafenib. Our findings may facilitate a better understanding of BRAFi resistance in thyroid carcinoma and introduce new potential therapeutic targets for thyroid cancer patients.

Conflict of Interest

The authors declare that there is no conflict of interest that could be perceived as prejudicing the impartiality of the research reported.

Funding

Appendix A. Supplementary data

Supplementary data related to this article can be found online at https://doi.org/10.1016/j.tranon.2019.10.007

References

[1] Siegel RL, Miller KD and Jemal A (2018). Cancer statistics, 2018. *CA Cancer J Clin* **68**, 7−30. https://doi.org/10.3322/caac.21442.

[2] Chmielik E, Rusinek D, Oczko-Wojciechowska M, Jarzab M, Krajewska J, Czarniecka A and Jarzab B (2018). Heterogeneity of thyroid cancer. *Pathobiology* **85**, 117−129. https://doi.org/10.1159/000486422.

[3] Smallridge RC, Ain KB, Asa SL, Bible KC, Brierley JD, Burman KD, Kebebew E, Lee NY, Nikiforov YE and Rosenthal MS, et al (2012). American Thyroid Association guidelines for management of patients with anaplastic thyroid cancer. *Thyroid* **22**, 1104−1139. https://doi.org/10.1089/thy.2012.0302.

[4] Ito Y, Miyauchi A, Ito M, Yabuta T, Masuoka H, Higashiyama T, Fukushima M, Kobayashi K, Kihara M and Miya A (2014). Prognosis and prognostic factors of differentiated thyroid carcinoma after the appearance of metastasis refractory to radioactive iodine therapy. *Endocr J* **61**, 821−824.

[5] Landa I, Ibrahimpasic T, Boucai L, Sinha R, Knauf JA, Shah RH, Dogan S, Ricarte-Filho JC, Krishnamoorthy GP and Xu B, et al (2016). Genomic and transcriptomic hallmarks of poorly differentiated and anaplastic thyroid cancers. *J Clin Investig* **126**, 1052−1066. https://doi.org/10.1172/jci85271.

[6] Integrated genomic characterization of papillary thyroid carcinoma. *Cell* **159**, 676−690. https://doi.org/10.1016/j.cell.2014.09.050.

[7] McArthur GA, Chapman PB, Robert C, Larkin J, Haanen JB, Dummer R, Ribas A, Hogg D, Hamid O and Ascierto PA, et al (2014). Safety and efficacy of vemurafenib in BRAF(V600E) and BRAF(V600K) mutation-positive melanoma (BRIM-3): extended follow-up of a phase 3, randomised, open-label study. *Lancet Oncol* **15**, 323−332. https://doi.org/10.1016/s1470-2045(14)70012-9.

[8] Kim KB, Cabanillas ME, Lazar AJ, Williams MD, Sanders DL, Ilagan JL, Nolop K, Lee RJ and Sherman SI (2013). Clinical responses to vemurafenib in patients with metastatic papillary thyroid cancer harboring BRAF(V600E) mutation. *Thyroid* **23**, 1277−1283. https://doi.org/10.1089/thy.2013.0057.

[9] Brose MS, Cabanillas ME, Cohen EE, Wirth LJ, Riehl T, Yue H, Sherman SI and Sherman EJ (2016). Vemurafenib in patients with BRAF(V600E)-positive metastatic or unresectable papillary thyroid cancer refractory to radioactive iodine: a non-randomised, multicentre, open-label, phase 2 trial. *Lancet Oncol* **17**, 1272−1282. https://doi.org/10.1016/s1470-2045(16)30166-8.

[10] Hyman DM, Puzanov I, Subbiah V, Faris JE, Chau I, Blay JY, Wolf J, Raje NS, Diamond EL and Hollebecque A, et al (2015). Vemurafenib in multiple nonmelanoma cancers with BRAF V600 mutations. *N Engl J Med* **373**, 726−736. https://doi.org/10.1056/NEJMoa1502309.

[11] Montero-Conde C, Ruiz-Llorente S, Dominguez JM, Knauf JA, Viale A, Sherman EJ, Ryder M, Ghossein RA, Rosen N and Fagin JA (2013). Relief of feedback inhibition of HER3 transcription by RAF and MEK inhibitors attenuates their antitumor effects in BRAF-mutant thyroid carcinomas. *Cancer Discov* **3**, 520−533. https://doi.org/10.1158/2159-8290.cd-12-0531.

[12] Gunda V, Bucur O, Varnau J, Vanden Borre P, Bernasconi MJ, Khosravi-Far R and Parangi S (2014). Blocks to thyroid cancer cell apoptosis can be overcome by inhibition of the MAPK and PI3K/AKT pathways. *Cell Death Dis* **5**, e1104. https://doi.org/10.1038/cddis.2014.78.

[13] Cheng L, Jin Y, Liu M, Ruan M and Chen L (2017). HER inhibitor promotes BRAF/MEK inhibitor-induced redifferentiation in papillary thyroid cancer harboring BRAFV600E. *Oncotarget* **8**, 19843−19854. https://doi.org/10.18632/oncotarget.15773.

[14] Wang W, Kang H, Zhao Y, Min I, Wyrwas B, Moore M, Teng L, Zarnegar R, Jiang X and Fahey 3rd TJ (2017). Targeting autophagy sensitizes BRAF-mutant thyroid cancer to vemurafenib. *J Clin Endocrinol Metab* **102**, 634−643. https://doi.org/10.1210/jc.2016-1999.

[15] Kim KS, Min JK, Liang ZL, Lee K, Lee JU, Bae KH, Lee MH, Lee SE, Ryu MJ and Kim SJ, et al (2012). Aberrant l1 cell adhesion molecule affects tumor behavior and chemosensitivity in anaplastic thyroid carcinoma. *Clin Cancer Res* **18**, 3071−3078. https://doi.org/10.1158/1078-0432.ccr-11-2757.

[16] Min IM, Shevlin E, Vedvyas Y, Zaman M, Wyrwas B, Scognamiglio T, Moore MD, Wang W, Park S and Park S, et al (2017). Therapy targeting ICAM-1 eliminates advanced human thyroid tumors. *Clin Cancer Res* **23**, 7569−7583. https://doi.org/10.1158/1078-0432.ccr-17-2008.

[17] Yang AH, Chau YP, Lee CH, Chen JY, Chen JY, Ke CC and Liu RS (2013). The influence of neural cell adhesion molecule isoform 140 on the metastasis of thyroid carcinoma. *Clin Exp Metastasis* **30**, 299−307. https://doi.org/10.1007/s10585-012-9537-6.

[18] Gorka B, Skubis-Zegadlo J, Mikula M, Bardadin K, Paliczka E and Czarnocka B (2007). NrCAM, a neuronal system cell-adhesion molecule, is induced in papillary thyroid carcinomas. *Br J Canc* **97**, 531−538. https://doi.org/10.1038/sj.bjc.6603915.

[19] Eke I and Cordes N (2015). Focal adhesion signaling and therapy resistance in cancer. *Semin Cancer Biol* **31**, 65−75. https://doi.org/10.1016/j.semcancer.2014.07.009.

[20] Banks RE, Gearing AJ, Hemingway IK, Norfolk DR, Perren TJ and Selby PJ (1993). Circulating intercellular adhesion molecule-1 (ICAM-1), E-selectin and vascular cell adhesion molecule-1 (VCAM-1) in human malignancies. *Br J Canc* **68**, 122−124.

[21] Shioi K, Komiya A, Hattori K, Huang Y, Sano F, Murakami T, Nakaigawa N, Kishida T, Kubota Y and Nagashima Y, et al (2006). Vascular cell adhesion molecule 1 predicts cancer-free survival in clear cell renal carcinoma patients. *Clin Cancer Res* **12**, 7339−7346. https://doi.org/10.1158/1078-0432.ccr-06-1737.

[22] Alexiou D, Karayiannakis AJ, Syrigos KN, Zbar A, Sekara E, Michail P, Rosenberg T and Diamantis T (2003). Clinical significance of serum levels of E-selectin, intercellular adhesion molecule-1, and vascular cell adhesion molecule-1 in gastric cancer patients. *Am J Gastroenterol* **98**, 478−485. https://doi.org/10.1111/j.1572-0241.2003.07259.x.

[23] Dymicka-Piekarska V, Guzinska-Ustymowicz K, Kuklinski A and Kemona H (2012). Prognostic significance of adhesion molecules (sICAM-1, sVCAM-1) and VEGF in colorectal cancer patients. *Thromb Res* **129**, e47−e50. https://doi.org/10.1016/j.thromres.2011.12.004.

[24] Kobawala TP, Trivedi TI, Gajjar KK, Patel DH, Patel GH and Ghosh NR (2016). Significance of TNF-alpha and the adhesion molecules: L-selectin and VCAM-1 in papillary thyroid carcinoma. *J Thyroid Res* **2016**, 8143695. https://doi.org/10.1155/2016/8143695.

[25] Wang PC, Weng CC, Hou YS, Jian SF, Fang KT, Hou MF and Cheng KH (2014). Activation of VCAM-1 and its associated molecule CD44 leads to increased malignant potential of breast cancer cells. *Int J Mol Sci* **15**, 3560−3579. https://doi.org/10.3390/ijms15033560.

[26] Scalici JM, Thomas S, Harrer C, Raines TA, Curran J, Atkins KA, Conaway MR, Duska L, Kelly KA and Slack-Davis JK (2013). Imaging VCAM-1 as an indicator of treatment efficacy in metastatic ovarian cancer. *J Nucl Med* **54**, 1883−1889. https://doi.org/10.2967/jnumed.112.117796.

[27] Zhong S, Joung JG, Zheng Y, Chen YR, Liu B, Shao Y, Xiang JZ, Fei Z and Giovannoni JJ (2011). High-throughput illumina strand-specific RNA sequencing library preparation. *Cold Spring Harb Protoc* **2011**, 940−949. https://doi.org/10.1101/pdb.prot5652.

[28] Trapnell C, Hendrickson DG, Sauvageau M, Goff L, Rinn JL and Pachter L (2013). Differential analysis of gene regulation at transcript resolution with RNA-seq. *Nat Biotechnol* **31**, 46−53. https://doi.org/10.1038/nbt.2450.

[29] Chanvorachote P and Chunhacha P (2013). Caveolin-1 regulates endothelial adhesion of lung cancer cells via reactive oxygen species-dependent mechanism. *PLoS One* **8**, e57466. https://doi.org/10.1371/journal.pone.0057466.

[30] Hou CH, Yang RS and Tsao YT (2018). Connective tissue growth factor stimulates osteosarcoma cell migration and induces osteosarcoma metastasis by upregulating VCAM-1 expression. *Biochem Pharmacol* **155**, 71−81. https://doi.org/10.1016/j.bcp.2018.06.015.

[31] Jacamo R, Chen Y, Wang Z, Ma W, Zhang M, Spaeth EL, Wang Y, Battula VL, Mak PY and Schallmoser K, et al (2014). Reciprocal leukemia-stroma VCAM-1/VLA-4-dependent activation of NF-kappaB mediates chemoresistance. *Blood* **123**, 2691−2702. https://doi.org/10.1182/blood-2013-06-511527.

[32] Teppo HR, Soini Y and Karihtala P (2017). Reactive oxygen species-mediated mechanisms of action of targeted cancer therapy. *Oxid Med Cell Longev* **2017**, 1485283. https://doi.org/10.1155/2017/1485283.

[33] Byeon HK, Na HJ, Yang YJ, Kwon HJ, Chang JW, Ban MJ, Kim WS, Shin DY, Lee EJ and Koh YW, et al (2016). c-Met-mediated reactivation of PI3K/AKT signaling contributes to insensitivity of BRAF(V600E) mutant thyroid cancer to BRAF inhibition. *Mol Carcinog* **55**, 1678−1687. https://doi.org/10.1002/mc.22418.

[34] Tsumagari K, Abd Elmageed ZY, Sholl AB, Friedlander P, Abdraboh M, Xing M, Boulares AH and Kandil E (2015). Simultaneous suppression of the MAP kinase and NF-kappaB pathways provides a robust therapeutic potential for thyroid cancer. *Cancer Lett* **368**, 46−53. https://doi.org/10.1016/j.canlet.2015.07.011.

[35] Lehraiki A, Cerezo M, Rouaud F, Abbe P, Allegra M, Kluza J, Marchetti P, Imbert V, Cheli Y and Bertolotto C, et al (2015). Increased CD271 expression by the NF-kB pathway promotes melanoma cell survival and drives acquired resistance to BRAF inhibitor vemurafenib. *Cell Discov* **1**, 15030. https://doi.org/10.1038/celldisc.2015.30.

[36] Rice GE, Munro JM, Corless C and Bevilacqua MP (1991). Vascular and nonvascular expression of INCAM-110. A target for mononuclear leukocyte adhesion in normal and inflamed human tissues. *Am J Pathol* **138**, 385−393.

[37] Freedman AS, Munro JM, Rice GE, Bevilacqua MP, Morimoto C, McIntyre BW, Rhynhart K, Pober JS and Nadler LM (1990). Adhesion of human B cells to germinal centers in vitro involves VLA-4 and INCAM-110. *Science* **249**, 1030−1033.

[38] Schlesinger M and Bendas G (2015). Vascular cell adhesion molecule-1 (VCAM-1)–an increasing insight into its role in tumorigenicity and metastasis. *Int J Cancer* **136**, 2504−2514. https://doi.org/10.1002/ijc.28927.

[39] Lee CW, Lin CC, Luo SF, Lee HC, Lee IT, Aird WC, Hwang TL and Yang CM (2008). Tumor necrosis factor-alpha enhances neutrophil adhesiveness: induction of vascular cell adhesion molecule-1 via activation of Akt and CaM kinase II and modifications of histone acetyltransferase and histone deacetylase 4 in human tracheal smooth muscle cells. *Mol Pharmacol* **73**, 1454−1464. https://doi.org/10.1124/mol.107.038091.

[40] Amin MA, Haas CS, Zhu K, Mansfield PJ, Kim MJ, Lackowski NP and Koch AE (2006). Migration inhibitory factor up-regulates vascular cell adhesion molecule-1 and intercellular adhesion molecule-1 via Src, PI3 kinase, and NFkappaB. *Blood* **107**, 2252−2261. https://doi.org/10.1182/blood-2005-05-2011.

[41] Hertzman Johansson C and Egyhazi Brage S (2014). BRAF inhibitors in cancer therapy. *Pharmacol Ther* **142**, 176−182. https://doi.org/10.1016/j.pharmthera.2013.11.011.

[42] Guo C, Yang M, Jing L, Wang J, Yu Y, Li Y, Duan J, Zhou X, Li Y and Sun Z (2016). Amorphous silica nanoparticles trigger vascular endothelial cell injury through apoptosis and autophagy via reactive oxygen species-mediated MAPK/Bcl-2 and PI3K/Akt/mTOR signaling. *Int J Nanomed* **11**, 5257−5276. https://doi.org/10.2147/ijn.s112030.

[43] Lin YT, Chen LK, Jian DY, Hsu TC, Huang WC, Kuan TT, Wu SY, Kwok CF, Ho LT and Juan CC (2019). Visfatin promotes monocyte adhesion by upregulating ICAM-1 and VCAM-1 expression in endothelial cells via activation of p38-PI3K-Akt signaling and subsequent ROS production and IKK/NF-kappaB activation. *Cell Physiol Biochem* **52**, 1398−1411. https://doi.org/10.33594/000000098.

[44] Notarangelo T, Sisinni L, Condelli V and Landriscina M (2017). Dual EGFR and BRAF blockade overcomes resistance to vemurafenib in BRAF mutated thyroid carcinoma cells. *Cancer Cell Int* **17**, 86. https://doi.org/10.1186/s12935-017-0457-z.

[45] Huang J, Zhang J, Li H, Lu Z, Shan W, Mercado-Uribe I and Liu J (2013). VCAM1 expression correlated with tumorigenesis and poor prognosis in high grade serous ovarian cancer. *Am J Transl Res* **5**, 336−346.

[46] Tumor endothelial notch signaling drives metastasis via VCAM1. *Cancer Discov* **7**, Of11. https://doi.org/10.1158/2159-8290.cd-rw2017-041.

[47] Tai HC, Chang AC, Yu HJ, Huang CY, Tsai YC, Lai YW, Sun HL, Tang CH and Wang SW (2014). Osteoblast-derived WNT-induced secreted protein 1 increases VCAM-1 expression and enhances prostate cancer metastasis by down-regulating miR-126. *Oncotarget* **5**, 7589−7598. https://doi.org/10.18632/oncotarget.2280.

[48] Rice GE and Bevilacqua MP (1989). An inducible endothelial cell surface glycoprotein mediates melanoma adhesion. *Science* **246**, 1303−1306.

[49] Chen Q, Zhang XH and Massague J (2011). Macrophage binding to receptor VCAM-1 transmits survival signals in breast cancer cells that invade the lungs. *Cancer Cell* **20**, 538−549. https://doi.org/10.1016/j.ccr.2011.08.025.

[50] Newell DR (2001). Flasks, fibres and flanks–pre-clinical tumour models for predicting clinical antitumour activity. *Br J Canc* **84**, 1289−1290. https://doi.org/10.1054/bjoc.2001.1797.

[51] Gao H, Korn JM, Ferretti S, Monahan JE, Wang Y, Singh M, Zhang C, Schnell C, Yang G and Zhang Y, et al (2015). High-throughput screening using patient-derived tumor xenografts to predict clinical trial drug response. *Nat Med* **21**, 1318−1325. https://doi.org/10.1038/nm.3954.